Spatiotemporal sequence of Himalayan debris flow from analysis of high-frequency seismic noise

A. Burtin, L. Bollinger, Rodolphe Cattin, J. Vergne, J. L. Nabelek

Spatiotemporal sequence of Himalayan debris flow from analysis of high-frequency seismic noise

A. Burtin,[1,2] L. Bollinger,[2] R. Cattin,[3] J. Vergne,[4] and J. L. Nábělek[5]

Received 18 November 2008; revised 22 June 2009; accepted 10 July 2009; published 28 October 2009.

[1] During the 2003 summer monsoon, the Hi-CLIMB seismological stations deployed across the Himalayan Range detected bursts of high-frequency seismic noise that lasted several hours to days. On the basis of the cross correlation of seismic envelopes recorded at 11 stations, we show that the largest transient event on 15 August was located nearby a village partially destroyed on that day by a devastating debris flow. This consistency in both space and time suggests that high-frequency seismic noise analysis can be used to monitor debris flow generation as well as the evacuation of the sediment. A systematic study of one year of seismic noise, focusing on the detection of similar events, provides information on the spatial and temporal occurrence of mass movements at the front of the Himalayas. With a 50% probability of occurrence of a daily event, a total of 46 debris flows are seismically detected. Most of them were generated in regions of steep slopes, large gullies, and loose soils during the 2003 summer monsoon storms. These events are compared to local meteorological data to determine rainfall thresholds for slope failures, including the cumulative rainfall needed to bring the soil moisture content to failure capacity. The inferred thresholds are consistent with previous estimates deduced from soil studies as well as sediment supply investigations in the area. These results point out the potential of using seismic noise as a dedicated tool for monitoring the spatiotemporal occurrence of landslides and debris flows on a regional scale.

Citation: Burtin, A., L. Bollinger, R. Cattin, J. Vergne, and J. L. Nábělek (2009), Spatiotemporal sequence of Himalayan debris flow from analysis of high-frequency seismic noise, *J. Geophys. Res.*, *114*, F04009, doi:10.1029/2008JF001198.

1. Introduction

[2] Inventory maps of regional landslides and debris flows are a primary source of knowledge of these catastrophic phenomena. They enable us to investigate correlations between lithogeomorphological parameters and mass movements. However, these maps lack the time resolution needed to properly estimate event rates and denudation rates. This is principally due to an inadequate imagery database [*Brardinoni et al.*, 2003], possible repeated failures of a given landslide scar or, even less known, the healing of mass movements [e.g., *Reid*, 1998]. Although theory and experiments help to describe the mechanisms and the hydrologic conditions of debris flows induced by landslides [e.g., *Iverson and Reid*, 1997], they need to be compared with actual observations. Most geotechnical investigations are therefore complementary, usually constraining the time sequence of slope failure [e.g., *Angeli et al.*, 2000; *Malet et al.*, 2002]. These studies generally capture the principal physical processes at work, and help to constrain the local mass movement hazard. As they are primarily carried out in regions most strongly affected by landslides, geotechnical studies make a highly selected data set for landslide hazard assessment. There is therefore a need to develop in these high risk areas a systematic tool for monitoring the spatiotemporal structure of landsliding and debris flow at regional scale. In this regard, various landslide monitoring systems reviewed by *Itakura et al.* [2005] and *Arattano and Marchi* [2008] have been developed, including wire sensors, photocells, ultrasonic, infrasonic [*Zhang et al.*, 2004], and ground vibration sensors such as geophones, accelerometers, and velocimeters [e.g., *Marchi et al.*, 2002]. The purpose of this article is to further explore the potential of this last technique, using a nondedicated temporary seismic network to monitor the spatiotemporal structure of slope failure at a regional scale.

[3] The Himalayas are one of the most landslide prone regions of the world [e.g., *Shroder*, 1998], with hundreds of landslides triggered per summer monsoon season. It is a place of great potential for the monitoring of mass movements. In Nepal, slope failures strongly impact the economy, regularly affect roads and bridges, and cause more than 200 deaths each year [*Upreti and Dhital*, 1996]. Slope failures are also a dominant process of hill-

[1]Laboratoire de Géologie, École Normale Supérieure de Paris, CNRS, Paris, France.
[2]CEA, DAM, DIF, Arpajon, France.
[3]Géosciences Montpellier, Université Montpellier 2, CNRS, Montpellier, France.
[4]Institut de Physique du Globe de Strasbourg, UMR 7516, CNRS-ULP, Strasbourg, France.
[5]College of Oceanic and Atmospheric Sciences, Oregon State University, Corvallis, Oregon, USA.

0148-0227/09/2008JF001198

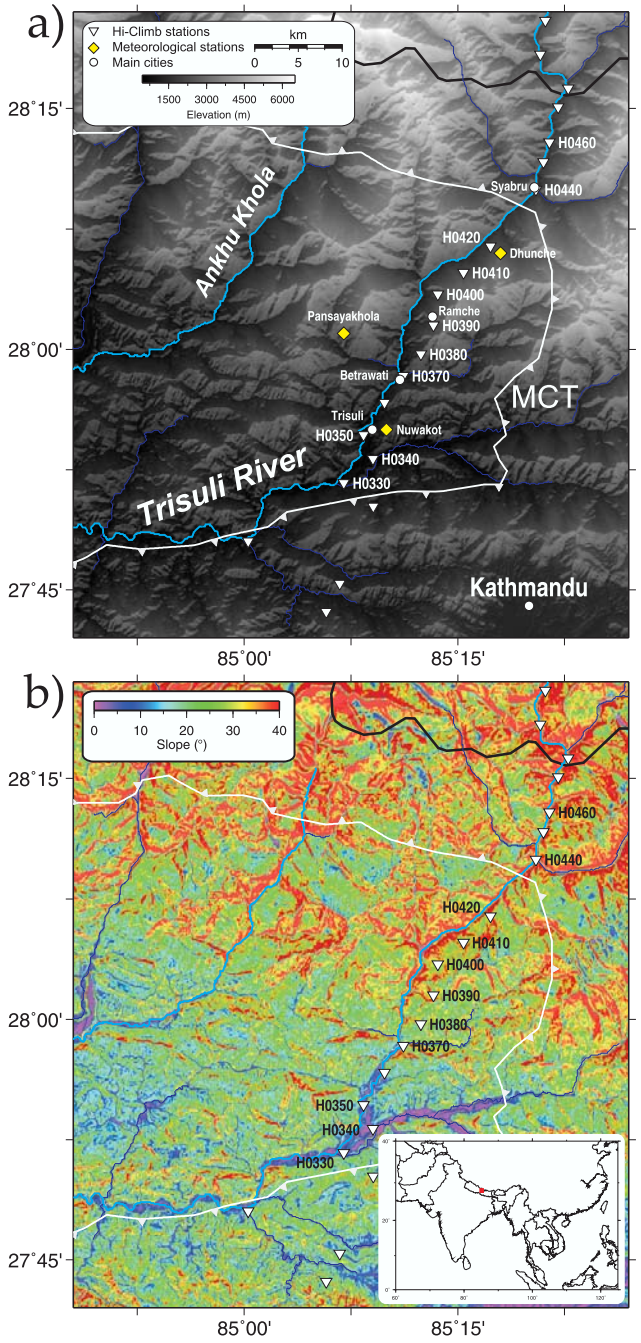

Figure 1. (a) Topographic map with the Hi-CLIMB seismological network, the meteorological stations from the Department of Hydrology, and Meteorology of Nepal used in this study as well as main cities. MCT refers to Main Central Thrust. (b) Slope map of the region with values given in degrees. (bottom right) Location of the study area in central Nepal (red mark in the global map).

slope denudation and a major source of sediment for rivers [e.g., *Burbank et al.*, 1996; *Attal and Lavé*, 2006]. Except for a few systematic landslide inventories [e.g., *Thouret*, 1983; *Marston et al.*, 1998] and geotechnical investigations of highly devastating events, most studies are confined to regions along major roads [e.g., *Dhital et al.*, 1991; *Hasegawa et al.*, 2008] or impacted populated areas [e.g., *Paul et al.*, 2000; *Dhital*, 2003; *Adhikari and Koshimizu*, 2005].

[4] Continuous monitoring by seismic networks in the afflicted areas presents an opportunity to record landslide-related signals. In 2003, several stations of the Hi-CLIMB network were deployed along the eastern bank of the Trisuli River (Figure 1). Ambient seismic noise analyses from Hi-CLIMB stations have already shown periodic features of high-frequency seismic noise [*Burtin et al.*, 2008]. Here, we focus on large bursts of seismic energy recorded at several stations along the profile. First, to validate our approach we use spectral analysis and a location method using cross correlation of seismic envelopes to demonstrate that the largest seismic event recorded on 15 August 2003 is associated with a large mass movement, the Ramche Debris Flow (named hereafter RDF). This debris flow claimed the lives of 45 people. We then extend the analysis over the 2003 monsoon period to detect the largest mass movements in the region. We investigate their distribution in time and space, and further constrain the rainfall threshold for landsliding in this area.

2. Data, Processing, and Regional Setting

[5] We analyze signals recorded by 11 seismological stations deployed during the Hi-CLIMB experiment (Table S1 of the auxiliary material), a passive seismic project dedicated to imaging lithospheric structures in Nepal and southern Tibet [*Hetényi*, 2007; *Nábělek et al.*, 2009].[1] The stations cross the Nepalese Himalayas from the foothills to the High Range at 3-km spacing. Stations H0330 to H0420, used for the study, are located in the Lesser Himalayas series, and consist of lower-grade metasediments [*Shrestha et al.*, 1985]. Farther north, stations H0440 and H0460 are on crystalline rock units of the higher Himalayas, which are mainly composed of gneisses and quartzites [*Upreti*, 1999]. Apart from technical issues, these stations operated continuously during the 2003 monsoon season. A multitaper method [*Thomson*, 1982; *Percival and Walden*, 1993] was used for spectral analysis of the continuous seismic recordings. Choosing a 5-min-long moving window with 50% overlap of the seismic records gives a good spectral resolution in the frequency range of interest (Figure 2).

[6] During the 2003 monsoon season, the H0410 spectrogram shows an increase of high-frequency seismic noise (>1 Hz) which is accompanied by the occurrences of sudden bursts of seismic energy over the 2–22 Hz frequency band (Figure 2a). The bursts are characterized by an increase of seismic energy that lasts less than a couple of hours followed by a gentle decrease. The dissipation of the energy can sometimes last up to several days before it reaches the ambient level prior to the burst event. These transient events of high-frequency seismic energy are well recorded on stations H0370 to H0410 but a single event is not always observed at every station. In a previous study [*Burtin et al.*, 2008], we have shown that, along the Trisuli River, human-induced seismic noise is low. North of H0410, we have

[1] Auxiliary materials are available in the HTML. doi:10.1029/2008JF001198.

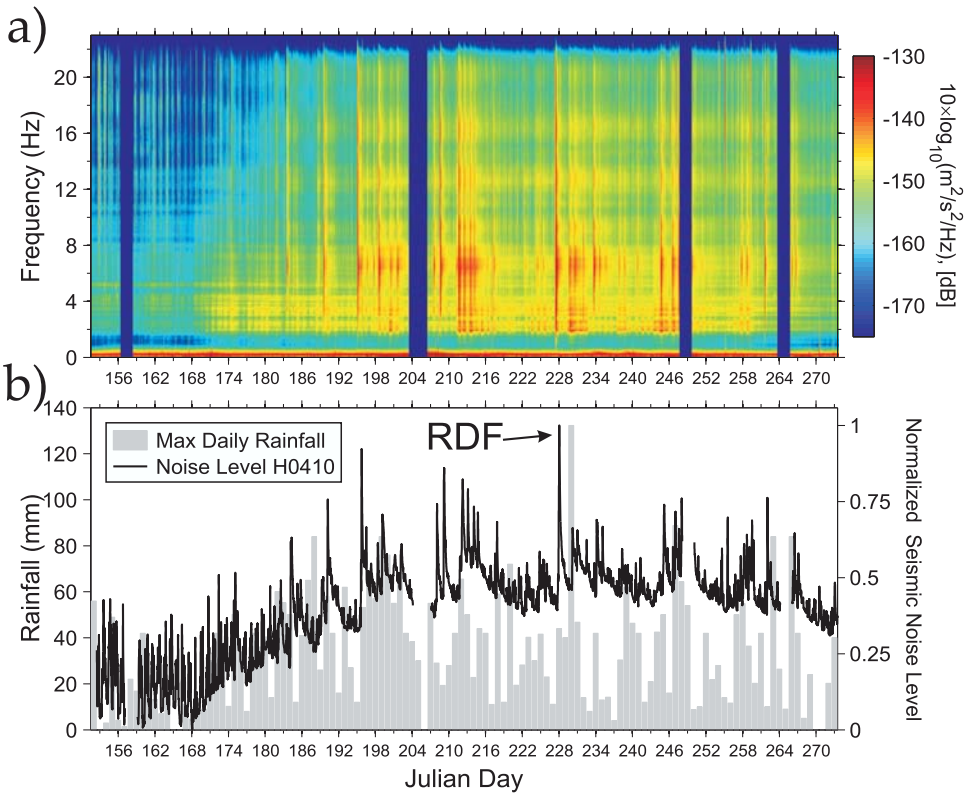

Figure 2. (a) Spectrogram at H0410 of the vertical component during the 2003 monsoon season (from Julian days 152 to 273 corresponding to 1 June 2003 to 30 September 2003). A multitaper method on time series of 5-min-length with 50% overlap is used for the computation of the spectral energy. The amplitude is given in decibel, red and blue colors stand for high and low energy, respectively. (b) Comparison of the 1-h smoothed mean seismic noise level (band 2–22 Hz) recorded at H0410 (black line) with the maximum daily rainfall measured by the meteorological stations from the Department of Hydrology and Meteorology of Nepal (Figure 1). Precipitation is given in mm and seismic energy is scaled on the rainfall and corresponds to a variation of 30 dB.

inferred a 24-h periodicity in the seismic noise which was primarily correlated with the river bed load transport, given the presence of a hysteresis curve between seismic noise level and water level. This conclusion has been recently supported by a study depicting a similar hysteresis curve between suspended sediment load and the water discharge in western Nepal [*Gabet et al.*, 2008].

[7] To highlight the nonperiodic transient events at H0410, we calculate the mean seismic energy in the 2–22 Hz frequency band. We then compare the average noise level with the rainfall observed along the Trisuli River at three meteorological stations from the Department of Hydrology and Meteorology (DHM) (Figure 2b and Appendix A). At the beginning of the rainy season (Julian day 164 to 181), the rise of seismic energy correlates with daily precipitation values in time. During the month of July (Julian day 182 to 212), this pattern is reproduced and the first transient events are detected and coincide with daily rainfall greater than 40 mm. Afterward, some discrepancies between both data sets begin to appear. Although episodes of heavy rainfall, >50 mm/day, are generally associated with sharp transient increases of high-frequency seismic noise, some transients also are observed for precipitation of 15 mm/day. Finally, during the waning of the summer monsoon a lower envelope of high-frequency seismic energy appears systematically larger than daily rainfall. This observation is consistent with ambient seismic noise generated by the Trisuli River due to the melting of snow and ice over the summer [*Burtin et al.*, 2008], punctuated by pulses of seismic energy linked to intense rainfall.

[8] At H0410, there were 46 bursts of high-frequency seismic noise with highly variable amplitudes and durations during the summer of 2003. Among these high-frequency seismic episodes, the strongest transient event observed at H0410 started on 15 August (Julian day 227). The event showed a peak amplitude equal to an increase of 15 dB that lasted more than three days at this seismological station. According to the *Kathmandu Post* [2003] and local inhabitants, a massive debris flow occurred on that day near the village of Ramche, close to H0390 (Figures 1 and 3). This suggests a correlation between the 15 August seismic event and the RDF.

3. Ramche Debris Flow Analyses

[9] Despite all the information concerning the RDF that has been collected from the inhabitants of Ramche and

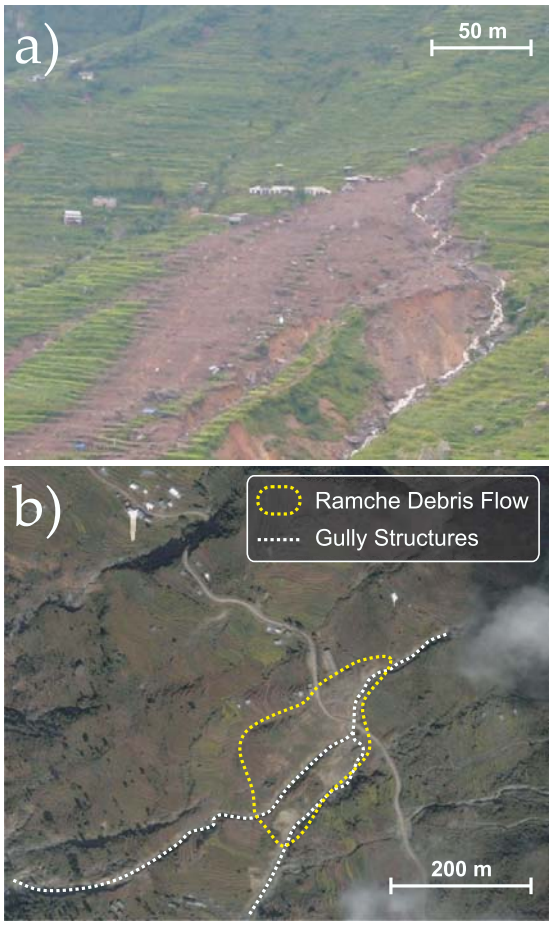

Figure 3. (a) Photograph of the Ramche Debris Flow (RDF) taken a few days after the event showing its deposition zone in the Ramche village. We estimate a minimum volume for the debris flow of 1.5×10^4 m^3 since a certain amount of debris reached the Trisuli River. (b) Digital Globe Quickbird image of the RDF acquired on 28 November 2004, 15 months after the debris flow.

newspapers, the initiation time of the slide is not well documented. We do know that destruction caused by the debris flow occurred around 2000 LT. Among the available Hi-CLIMB stations, H0390 was located only 400 m away from the RDF. Seismic data collected during this time period show important complexities (Figure 4). The signals recorded at stations nearest the RDF reveal the existence of at least three main peaks of amplitude, named hereafter P1, P2, and P3 for the first, second and third event, respectively. Each event lasts about 2 min and is separated from the others by about 25 min (Figure 4). Although we do not have any clear evidence, we propose that one or all of these peaks represent the seismic signal from the observed debris flow. To test this hypothesis, we attempt to seismically locate these three events. We use all the Hi-CLIMB stations at a distance <26 km from the RDF all of which clearly recorded the three events (Figure S1 of the auxiliary material).

3.1. Transient Events Location: Example of the RDF

[10] To locate an event, we extract for each of 3 components of a station a 2- to 4-min-long recording (depending on the complexity of the event) and roughly centered on the peak of amplitude. These time series are then band-pass filtered between 0.6 and 0.9 Hz, and an energy envelope is produced. At each station, the energy envelopes of the 3 components are summed and normalized. An example of the energy envelopes for event P3 of RDF is shown in Figure 5a. The chosen frequency band is used to efficiently isolate a seismic wave phase that can be coherently observed at numerous stations. A station not showing a clearly characteristic envelope and event is discarded. For example, stations H0340 and H0390 are discarded for the location of events P1 and P2, respectively. For each station couple we use a cross-correlation technique to calculate the best time delay between two energy envelopes. These delays are then processed to calculate the likely location of the event according to a probability density method.

[11] Since we know the occurrence of the RDF from field observations, we assume a location to produce a priori probability density that we define as

$$\rho_m(x,y) = e^{\left[-\frac{(x-x_0)^2+(y-y_0)^2}{2\sigma^2_{prior}}\right]}. \quad (1)$$

In this equation, x_0 and y_0 are the observed location coordinates of the RDF, x and y are the coordinates of a grid point and σ_{prior} is the error on the assumption, fixed at 10 km. For each station delay couple, we calculate the probability density that is described by this observation, using the following formulation:

$$\rho_d(x,y,V) = \sum_{i_1=1}^{N-1} \sum_{i_2=i_1+1}^{N} e^{\left[-\frac{\left(dt^{i_1,i_2}_{calc} - dt^{i_1,i_2}_{obs}\right)^2}{2\sigma_{dt}(V)^2}\right]}, \quad (2)$$

where i_1 and i_2 are the index number of stations, N is the number of available station time delay couples, and V is the velocity of envelope propagation in a tabular medium of constant velocity. Since this velocity is unknown, we seek the best solution for velocities ranging from 0.1 km/s to 4 km/s. In equation (2), dt_{obs} signifies the observed station delay while the calculated delay dt_{calc} is given as

$$dt^{i_1,i_2}_{calc}(x,y,V) = \frac{\sqrt{(x-x_{i_2})^2+(y-y_{i_1})^2} - \sqrt{(x-x_{i_2})^2+(y-y_{i_1})^2}}{V}.$$

To apply a constant spatial uncertainty despite different envelope velocities, we define in equation (2) the time error $\sigma_{dt}(V)$, a function of the velocity such that $\sigma_{dt} \times V = d_0$, where d_0 is fixed at 1 km.

[12] The final probability density is given by the relation

$$\rho_{final}(x,y,V) = \rho_m(x,y) \times \rho_d(x,y,V). \quad (3)$$

The best coherent localization and seismic wave propagation velocity are thus indicated by the maximum of the stacked envelope amplitudes. The results for the three events of RDF are shown in Figure 5.

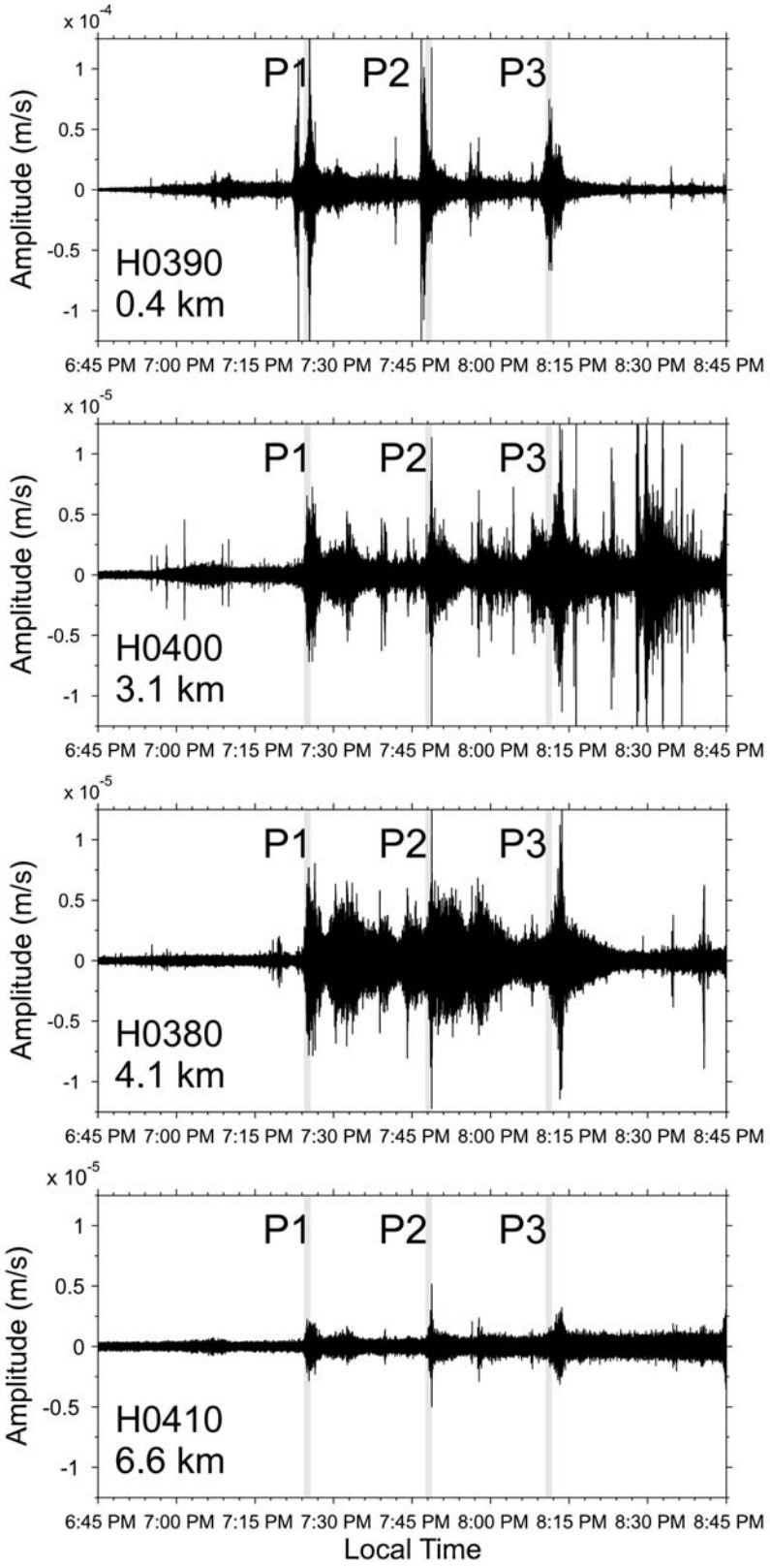

Figure 4. 2-h-long vertical seismograms recorded on 15 August 2003 at stations H0390, H0400, H0380, and H0410 from top to bottom and with an increased distance to the Ramche Debris Flow, respectively. The time is set in local time and the distance to the RDF is indicated beneath the station name. The data are band-pass filtered between 0.5 and 10 Hz. The amplitude is in m/s and is one order larger at H0390 than for the other three stations.

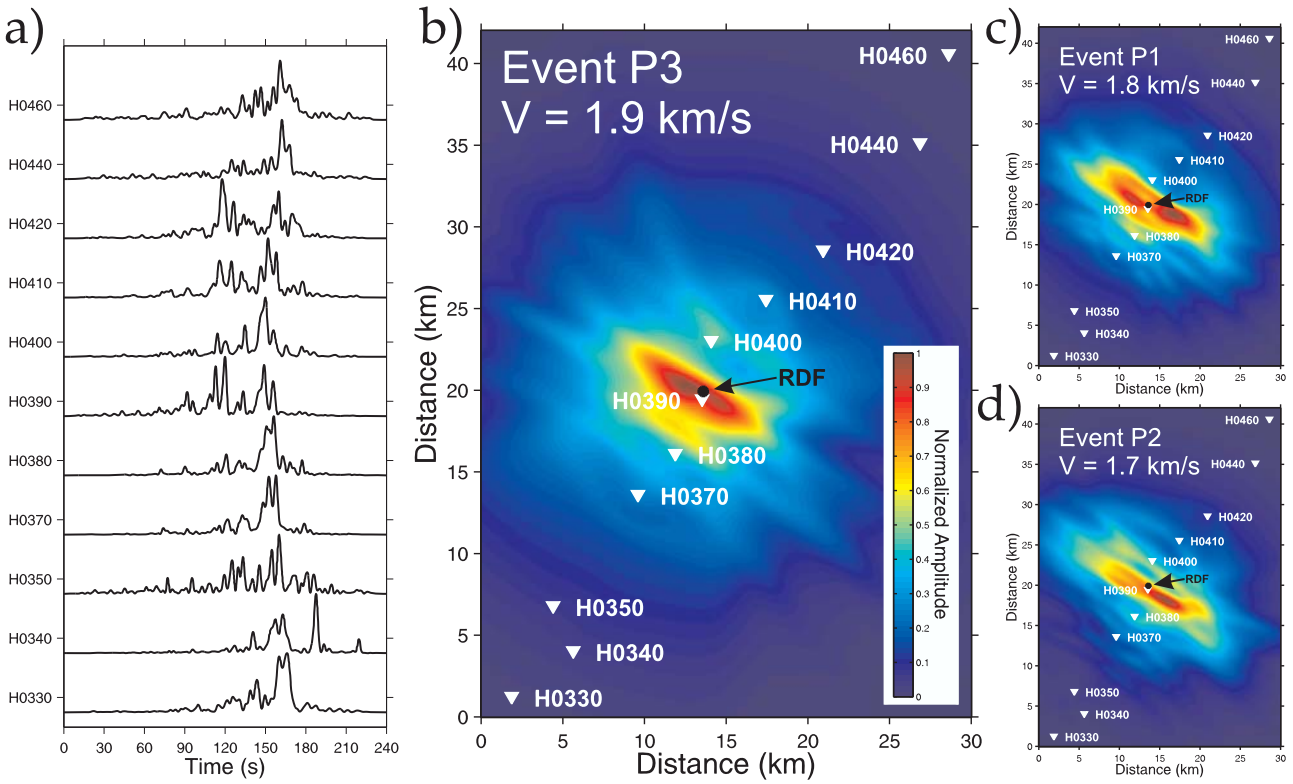

Figure 5. (a) Energy envelopes of the event P3 for stations H0330 to H0460 from bottom to top, respectively. The envelopes are calculated by the summation of the square amplitude envelope of each component at a station. These data are used to compute the arrival time delays at stations and to locate the event. The amplitudes are normalized to unit amplitude. (b) Best solution for the event P3 at an envelope velocity of 1.9 km/s. Seismic velocities explored for the localization range from 0.1 to 4 km/s. (c and d) Best solution for events P1 and P2, respectively. The color scale is similar for each coherence map. The station location is indicated with the inverse white triangle, and the location of the RDF from field observations is marked with a black dot.

[13] The time delay migration of the three events shows regions of increased coherence that merge as the velocity is increased (Movie S1 of the auxiliary material). Upon reaching the maximum amplitude we obtain the most likely location and the best envelope velocity estimate. As this velocity continues to increase, the area of strong coherence changes only slightly while the amplitude decreases, giving to these solutions lower probability. The best solutions for the three events (P1, P2, and P3) are all located near station H0390 (Figure 5) and near the RDF. The best estimated seismic group velocities are about 1.8 km/s. Although it is not obvious which event is associated with the RDF, P3 has a solution that is closest to the location of the RDF. These locations are strongly influenced by the linear geometry of the Hi-CLIMB array. Since the seismic network is distributed essentially along a north-south line, the resolution along the array is well defined whereas the resolution perpendicular to the array is not.

[14] To test the robustness of our results from the RDF location and to justify using a priori information, we have conducted several sensitivity tests. In Figure 6, we show the results of the location of event P3 without any a priori information. The best solution found for an envelope velocity of 1 km/s is located on the western border of the explored area (Figure 6a). This solution reflects the strong influence of the geometry of the Hi-CLIMB array. During the migration of the observed time delays, the solution that corresponds to a single delay between two stations follows a hyperbola, which remains widely open at low velocities. Since the seismic array is a line, the different hyperbolas merge in the lateral regions and produce some coherence. Such an effect is removed when the migration velocity increases. The coherence map for an envelope velocity of 1.9 km/s is equivalent to the one found using a priori information. The representation of the maximum of the coherence map for each velocity, with or without a priori information, results in a similar conclusion. At high velocity the maximum of coherence follows in both cases the same trend, whereas at low velocity discrepancies are observed (Figure 6c). The use of an a priori probability density is helpful to suppress the geometrical effect induced by Hi-CLIMB network and with σ_{prior} increasing until 25 km, we infer similar results. Finally, if the seismic array had been deployed with lateral extensions along the Himalayan arc, the use of a priori information probably would have been unnecessary.

[15] Despite the remaining uncertainty on the source location, we confirm that the sources of the three main

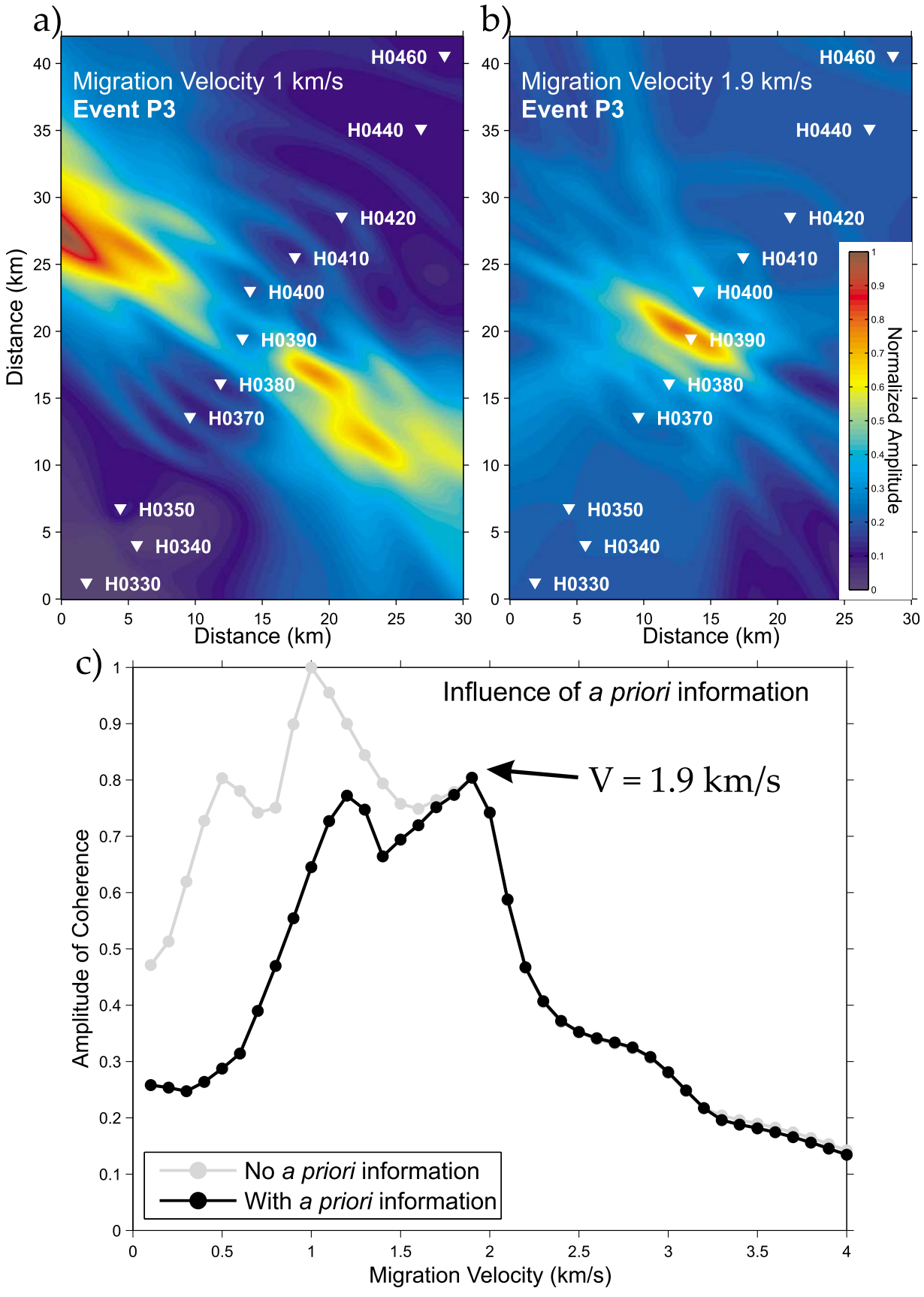
a)
Migration Velocity 1 km/s
Event P3
H0460
H0440
H0420
H0410
H0400
H0390
H0380
H0370
H0350
H0340
H0330
Distance (km)
Distance (km)
b)
Migration Velocity 1.9 km/s
Event P3
Normalized Amplitude
c)
Influence of a priori information
V = 1.9 km/s
Amplitude of Coherence
No a priori information
With a priori information
Migration Velocity (km/s)

Figure 6

peaks of energy are within the gullies that were affected by the RDF (Figure 3). Our result also illustrates the potential of using seismic signals for estimating the location of rapid mass movements.

3.2. Further Analyses of the High-Frequency Seismic Noise Generated by the RDF

[16] The seismic noise level associated with the RDF was well above its mean monsoon level over the entire high-frequency band during the energy burst generated between 1800 and 2000 LT (Figure 7). This burst was related to the three main events presented above (referred as P1, P2 and P3). Following these events and up to one day later, the ambient seismic noise at high frequencies remained larger than prior to the debris flow. H0390 exhibited a noise level 10 dB and 5 dB greater than the initial level 5 and 20 h later, respectively. Furthermore, the higher frequencies involved in the energy burst took longer time to return to their former level than the lower frequencies (Figure 7b). The seismic noise spectrum, almost flat in the 2–22 Hz band during the RDF, depicted more high frequencies in the following hours.

[17] The same analysis conducted on H0410 also reveals a large increase of the high-frequency seismic noise level with a significantly different time history compared to H0390 (Figure 8). Although, P1, P2 and P3 are clearly identified at H0410 (Figure 4), the main peak of energy at this station occurs 2 h later. The spectral characteristics of this event are similar to those of the one at H0390 and therefore may indicate a similar source mechanism, suggesting another debris flow may have been triggered near H0410 on the same night. In addition, two other bursts of high-frequency seismic noise are identified two days after the RDF (Figure 8b). Such events of long duration high-frequency seismic noise are occasionally detected from stations H0370 and H0400. Nearby gullies with landslide scars are clearly visible on ASTER satellite imagery acquired in the region after the 2003 monsoon (Figure 9). Were these gullies all activated during the 2003 monsoon season? Did they produce rapid landslides and debris flows? To answer, we systematically applied the methodology described in the RDF study to all other energy bursts of similar characteristics recorded by the array in this region.

4. Debris Flow Data Set

[18] Our analysis identifies 46 distinct large events along the seismic network, from stations H0370 to H0410, and between June and September 2003.

4.1. Spatial Pattern

[19] All sources of the detected transient events appear to coincide with zones densely affected by landslide scars and debris flow gullies visible in Figure 9, between H0370 and H0410. This area corresponds to a region of steep slopes at the front of the Himalayan High Range, within the Lesser Himalayan series. Further north, within the High Himalayan Crystalline series, the slope distribution remains similar (Figure 1b). However, no transient event equivalent to these bursts of high-frequency seismic noise occurred during 2003. These results confirm the observations made in the same region by *Thouret* [1983] and *Marston et al.* [1998] showing that the number of slope failures is greater below the Main Central Thrust in the Lesser Himalayas than above. This behavior might be controlled by lithology, regolith characteristics (controlled, in general, by altitude and vegetation) and/or rain shadow.

[20] Although stations between H0330 and H0350 clearly recorded the RDF events (in the 0.6–0.9 Hz frequency band) and in spite of their low ambient seismic noise level (−148 dB in the 2–22 Hz band and only moderate anthropogenic perturbations) these stations did not detect any local transient events south of H0370. Between H0420 and H0460, the mean seismic noise level of −143 dB is larger than at H0410 with a level of −153 dB but this should not prevent us from detecting RDF-type events since the peak of energy from RDF at 8 km is equal to −140 dB. Thus, with a mean interstation distance of 5 km, we should be able to detect such events at one or more seismic stations.

4.2. Time Structure of the Mass Movement and Rainfall Thresholds

[21] *Thouret* [1983] worked during two monsoon seasons along the Ankhu Khola, in a valley parallel to and encompassing the same lithogeomorphological features as the Trisuli River instrumented here (Figure 1). He noticed that most mass movements coincide with the recrudescent spells of monsoon rainfall. He further observed that, despite their large volumes, sometimes as large as monsoon storms, the premonsoon rainfall events were not triggering mass movements. He attributed this fact to a threshold of plasticity and then liquidity of the soils, illustrating this hypothesis with several measurements for the degree of moisture of the soils through the rainy season. The soils he collected at several places encompass large moisture variations during the monsoon period, and require variable times to reach the failure threshold. These observations are well complemented by a sediment load study in a small river catchment located at the front of the western Nepal High Himalayas [*Gabet et al.*, 2004]. Their observations demonstrate that two different rainfall thresholds, a seasonal accumulation and a daily total, must be overcome before landslides can be initiated.

[22] Despite a limited number of transient events in our catalogue, 46 over one year, some characteristics of their time structure and soil conditions might be drawn and

Figure 6. (a) Best solution for the migration of the time delays from the event P3 with no a priori information. The best envelope velocity is found at 1 km/s, and the location of the event is on the western limit of the researched area. (b) Solution found for a migration velocity of 1.9 km/s and no a priori information. The coherence map is similar to the one found with the introduction of a priori information (Figure 5b). (c) Amplitude of the maximum of coherence for each migration velocity with no a priori information (gray curve) and with a priori information (black curve). The amplitude of the latter curve has been normalized to the value obtained for a velocity of 1.9 km/s in the case of no a priori information. The similarity between the curves is significant when the velocity increases and clearly reveals a geometrical effect of the array at low velocities.

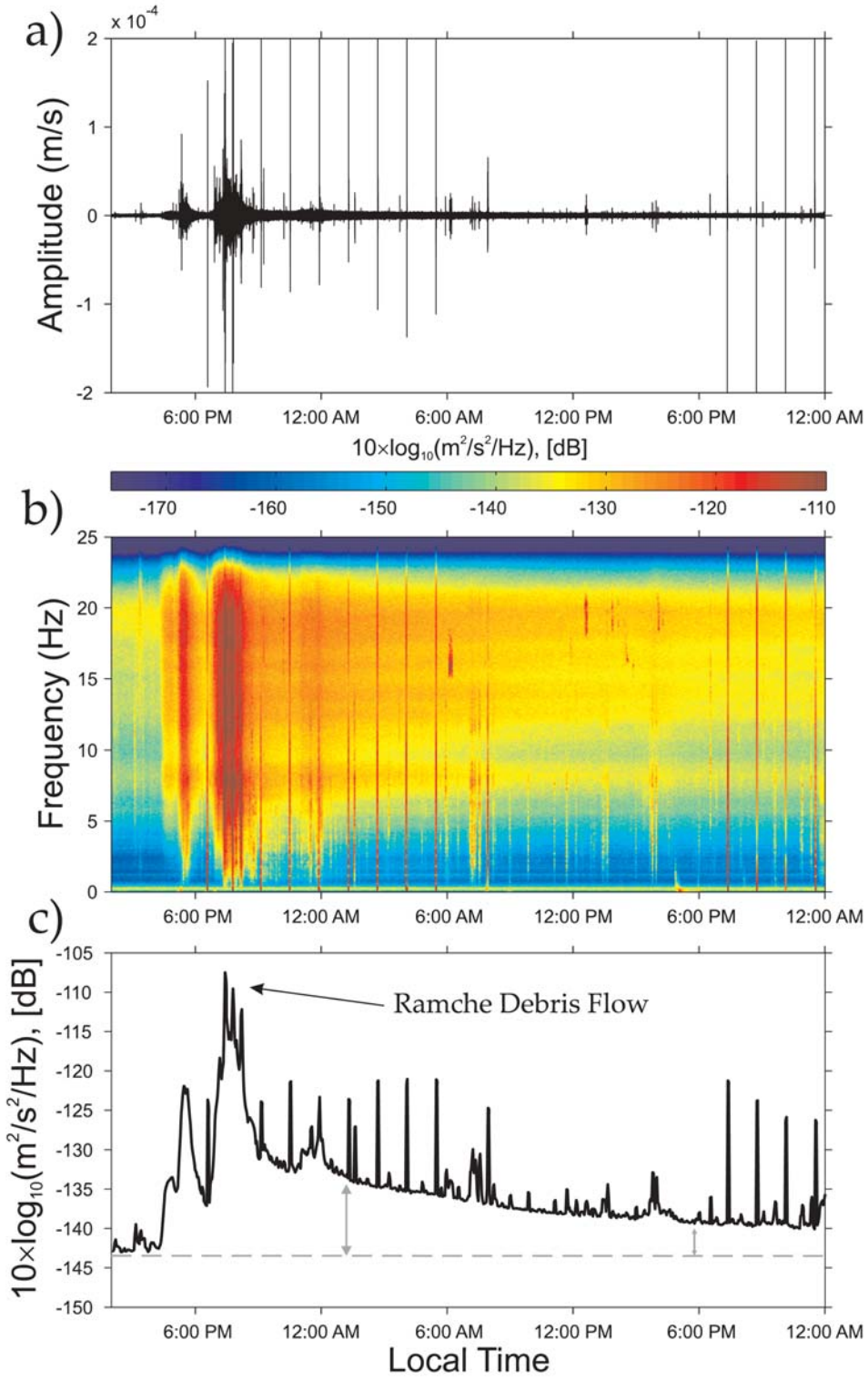

Figure 7. (a) Vertical seismogram recorded at H0390. The seismic signal is band-pass filtered between 0.1 and 20 Hz. The recording starts at 1400 LT on the 15 August 2003. (b) Spectrogram calculated from the vertical seismic recording at H0390 using a multitaper method with 50% overlap between time segments of 5 min. Amplitudes are given in decibels (dB); red and blue colors stand for high and low amplitudes, respectively. (c) The 1-h smoothed mean high-frequency seismic energy at H0390 for the vertical component (Figure 7b) in the 2–22 Hz frequency band. Amplitudes are given in dB.

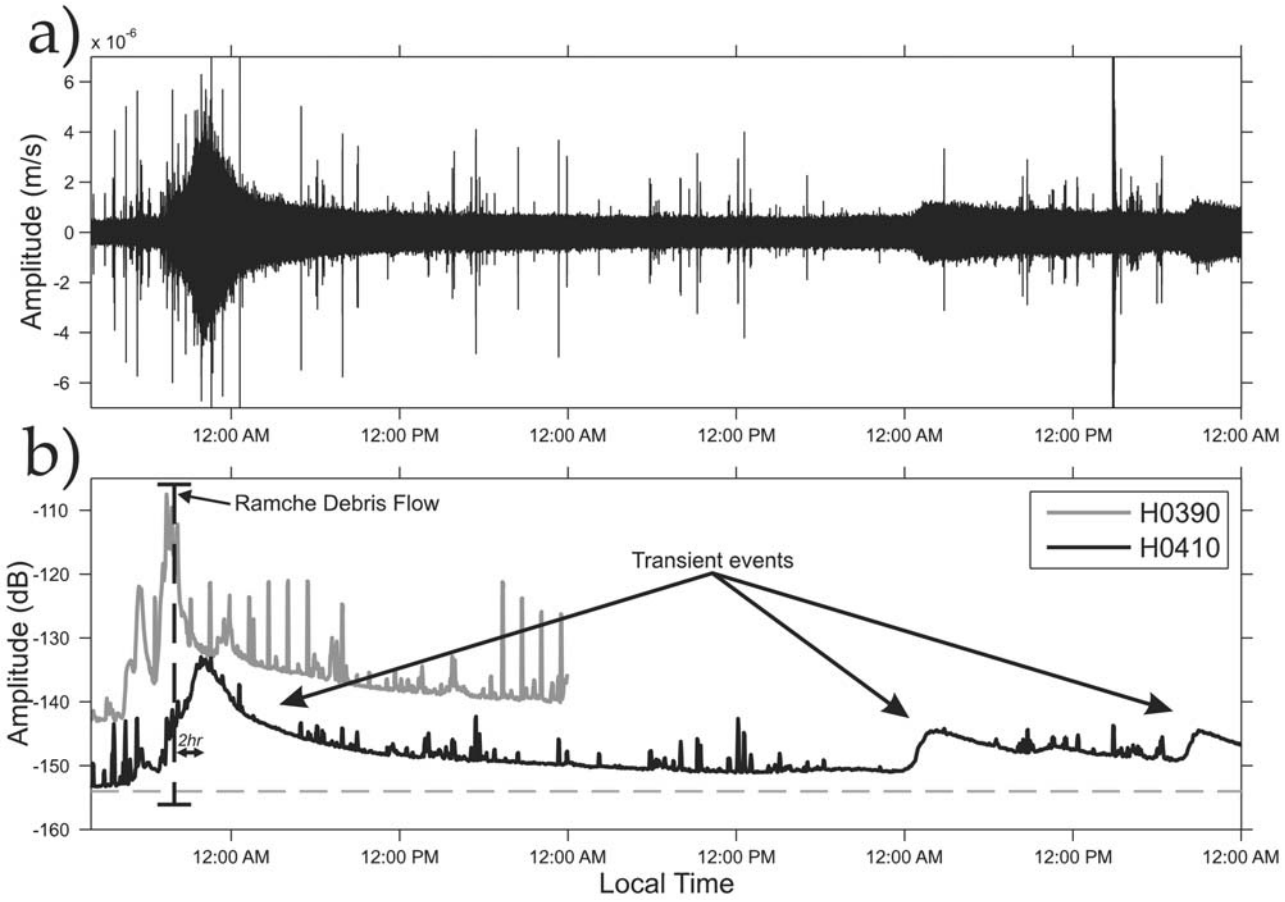

Figure 8. (a) Vertical seismogram recorded at H0410. The seismic signal is band-pass filtered between 0.1 and 20 Hz. The beginning of the recording starts at 1400 LT on the 15 August 2003. (b) Comparison of the 1-h smoothed mean high-frequency seismic energy in the 2–22 Hz frequency band at H0390 (gray) and H0410 (black) for the vertical component. Amplitudes are given in dB.

compared to those previous studies. First, most of the events occurred in the late evening or during the night, with 80% of the events detected between 1800 and 0400 LT and only two events between 0400 and 1200 LT (Table 1). This pattern is consistent with the mean diurnal cycle of rainfall observed for low and intermediate altitude stations at the front of the High Range [*Barros et al.*, 2000; *Ueno et al.*, 2001; *Bollasina et al.*, 2002] (Figure S2 of the auxiliary material). Second, all the events detected in 2003 happened during the summer monsoon season, between 23 June 2003 and 29 September 2003. Finally, the daily rainfall catalogue provided by the Department of Hydrology and Meteorology (DHM), Nepal at several meteorological stations along the seismic network allows us to estimate rainfall thresholds for debris flow triggering. Applying the same methodology as in the work of *Gabet et al.* [2004], Figure 10 shows the conditions under which events were detected at station H0410. We choose this station because it offers the best continuous data acquisition during the monsoon. It appears that the first transient event of seismic noise is observed after a rainfall accumulation of 450 mm while no event is detected during the monsoon onset. Afterward, a daily precipitation of about 10 mm seems to be required for triggering an event. The probability of occurrence of one event per day is as large as 50% and does not vary throughout the monsoon season (Figure 11). Our accumulated rainfall threshold is significantly different from the one observed in the Annapurna region (860 mm). However, this difference might be induced by several factors. First, in both studies, the origin time of the monsoon rainfall is arbitrary. Second, according to *Gabet et al.* [2004], this threshold is governed by regolith thickness and porosity, which might differ significantly between the two settings. A second threshold of about 10 mm, the amount of daily rainfall necessary to observe a debris flow after the accumulation threshold has been reached, is similar to the 11 mm estimated by *Gabet et al.* [2004]. This second threshold is poorly resolved by our observations since the meteorological data are sparse and show large spatial discrepancies. A minimum of accumulated rainfall is necessary to reach soil failure, whereas steep slopes and numerous rainstorms lead to hydrologic conditions that are probably beyond the daily threshold during monsoons (Figure 11). Therefore, antecedent rainfall seems to have a dominant role in triggering slope failures in the Himalayas of Nepal [*Dahal and Hasegawa*, 2008].

4.3. Threshold for Transient Event Detection

[23] The occurrence of transient events is correlated with the daily fluctuation of the seismic noise generated by the

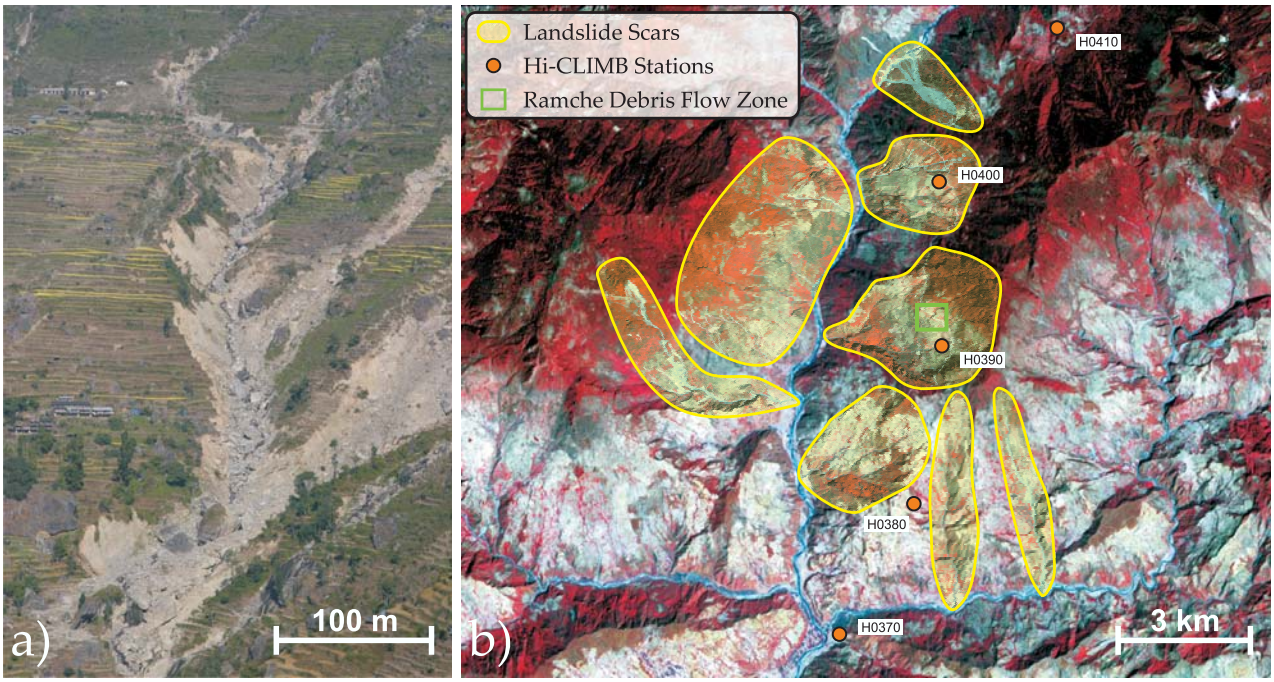

Figure 9. (a) Photograph of the gullies affected by the RDF which are close to station H0390. (b) ASTER color composition (RGB band L3B/2/1) of a scene acquired on 30 March 2001 corresponding to the highest landslide density area. The yellow zones mark the presence of important gully structures and landslide scars. At the front of the High Range, the Hi-CLIMB stations (orange dots) are located in the vicinity of these critical hillslopes. The green rectangle shows the region affected by the RDF.

Trisuli River [*Burtin et al.*, 2008]. Part of this seismic energy is produced by ground vibrations from bed load transport during increased river discharge. This increase in ambient seismic noise may thus prevent detection of small landslide events at night since the river reaches its maximum daily discharge and transport capacity over the monsoon season between 2000 and 0200 LT, inducing a maximum daily seismic noise level during this time window [*Burtin et al.*, 2008]. To investigate a possible link between the rainfall and the detection of bursts of high-frequency seismic noise, we determined the cumulative number of transient events as a function of their peak amplitude (Figure 12a). We fit the data to a relation for the magnitude-frequency distribution of transient events at H0410, where the number of events above a given magnitude is approximately linear. Nevertheless, this linear trend fails to explain the observed number of smaller events. From this analysis, we estimate a seismic noise threshold for the unbiased detection of a transient event to be at −143 dB. Then we recalculate the daily fluctuation for the occurrence of events using this threshold (Figure 12b). The correlation between precipitation and transient event occurrences is reproduced, implying a robust link between the two phenomena.

5. Generation of High-Frequency Seismic Noise and Debris Flow Implications

[24] During the RDF, a broad range of high frequencies (from 2 to 22 Hz) was excited at H0390 (Figure 7). Unfortunately, this frequency band corresponds to the band sometimes excited by bed load transport in the Trisuli River [*Burtin et al.*, 2008]. The seismic energy radiated during the RDF could either be produced by gullies activated by the RDF or mass wasting in the river. Uncertainties on the seismic location of the RDF do not enable us to discriminate between these scenarios. However, relative to nearby stations, the very high seismic noise level of −110 dB for the peak amplitude related to the event at H0390 (Figures 4 and 8) suggests that the origin of the seismic noise is in the near field of the station (few hundreds of meters). In addition, H0380 downstream the Trisuli River and at a shorter distance from the stream (Figure 1) records

Table 1. Occurrence Number of Transient Events as a Function of the Hour of the Day

	Time Occurrence of Transient Event											
Hour Gap	0–2	2–4	4–6	6–8	8–10	10–12	12–14	14–16	16–18	18–20	20–22	22–24
Occurrences	9	6	1	1	0	0	0	5	2	2	10	10

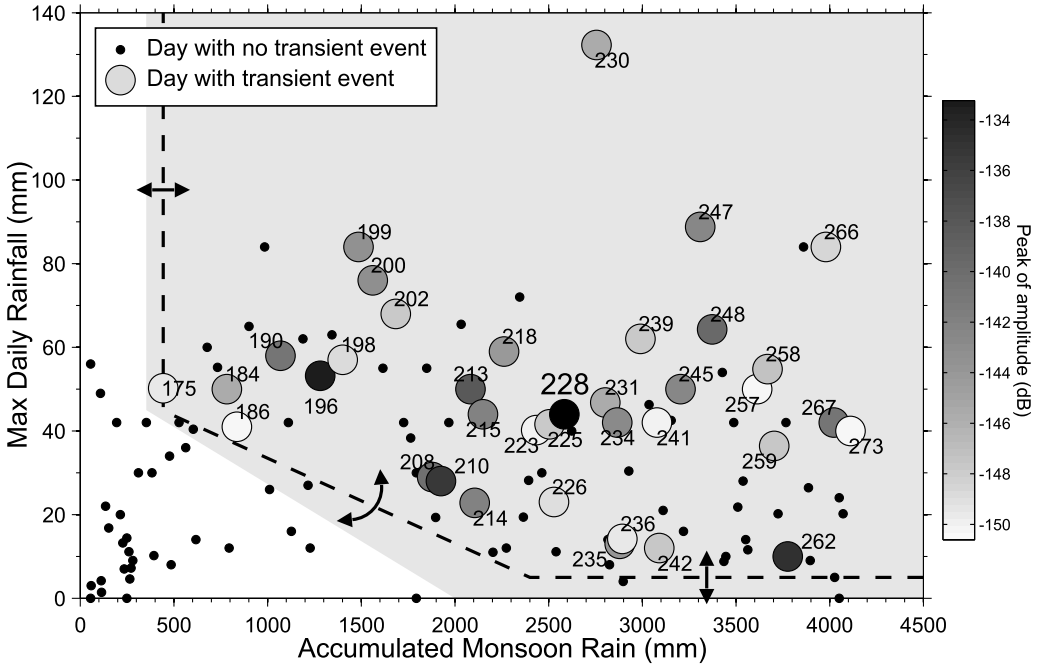

Figure 10. Rainfall thresholds for the occurrence of transient events. The shaded area delineates the rainfall values that may trigger a transient event, inspired from *Gabet et al.* [2004]. The dashed line delineates our preferred envelope of occurrences, whereas the double arrows qualitatively illustrate the range of uncertainties given on the envelope position according to the resolution of the meteorological data and the number of samples. Each dot marks the maximum daily rainfall as a function of the accumulated monsoon rain from the data represented in Figure 2b (see text for precisions). Small black dots stand for the days with no observed transient event and the large dots represent the days where at least one transient event is detected and their color mark the peak amplitude of the event in dB. Since the precipitation rate is daily acquired in the morning (around 0900 LT), we associate to this value the transient events that happened the last 24 h.

a seismic signal of 1 order lower magnitude than H0390 (Figure 4). These observations favor a local source of seismic noise, such as moving rock debris within the gullies. The materials supplied by the RDF are composed of rocks showing a wide range of sizes up to a decameter (Figures 3 and 9). The movement of such rocks has been reported to individually generate high-frequency seismic noise [*Huang et al.*, 2007]. This experimental study demonstrated that seismic frequencies excited by ground vibrations from rock motions are related to the object size, large boulders generating lower frequencies than small boulders. This observation could explain the time structure of the H0390 spectrogram on 15–16 August (Figure 7b). A low-frequency band of 2–5 Hz is excited during a period of only a few hours after the RDF, whereas a higher-frequency band, e.g., 18–21 Hz, still remains 30 h later at a higher noise level than prior to the event. Furthermore, and as discussed in section 3.2, the decay of seismic energy is more rapid at low frequency. This evidence is consistent with bed load transport in the gullies. Indeed minutes after the RDF, the supply of debris to the gully and the supply of water from rain and groundwater are apparently sufficient to exceed a critical shear stress competent to transport coarse sizes of sediments [e.g., *du Boys*, 1879; *Shields*, 1936]. With the end of precipitation the streamflow declines resulting in the cessation of movement of the largest sediment sizes. Thus we observe a more rapid decrease of the energy at low frequencies in response to a possible size-selective transport.

[25] Furthermore, the daily variability of the seismic transient events correlates with the daily evolution of monsoon rainfall along the Himalayan Arc, where 80% of events occurred during the peak of precipitation from 1800 to 0400 LT. The coherence between data sets reinforces the role of water supply for the generation of ground vibrations induced by bed load motion. Contrary to the Trisuli River, which has a water supply coming from both the melting of snow or glaciers and rainfall, the gullies are fed only by strong monsoon rainfall. The steep slopes and large amounts of water result in a highly turbulent stream that can mobilize a broad fraction of bed load. From these coherences, we conclude that superposed with the river seismic noise the high-frequency transient events lasting several hours to days and recorded by the Hi-CLIMB stations at the front of the High Range are an indicator of sediment transport in gullies. These bursts of high-frequency energy are consistent with the pulsatory nature of sediment load in a river from hillslope inputs [e.g., *Hovius et al.*, 2000]. Along the Trisuli River such sediment supplies may contribute to the evolution of fluvial networks by introducing efficient tools for bedrock incision. In the region where we observed the transient events, high incision rates (>5 mm/yr) have been inferred by *Lavé and Avouac* [2001]. Although ephemeral, the sediment transport within

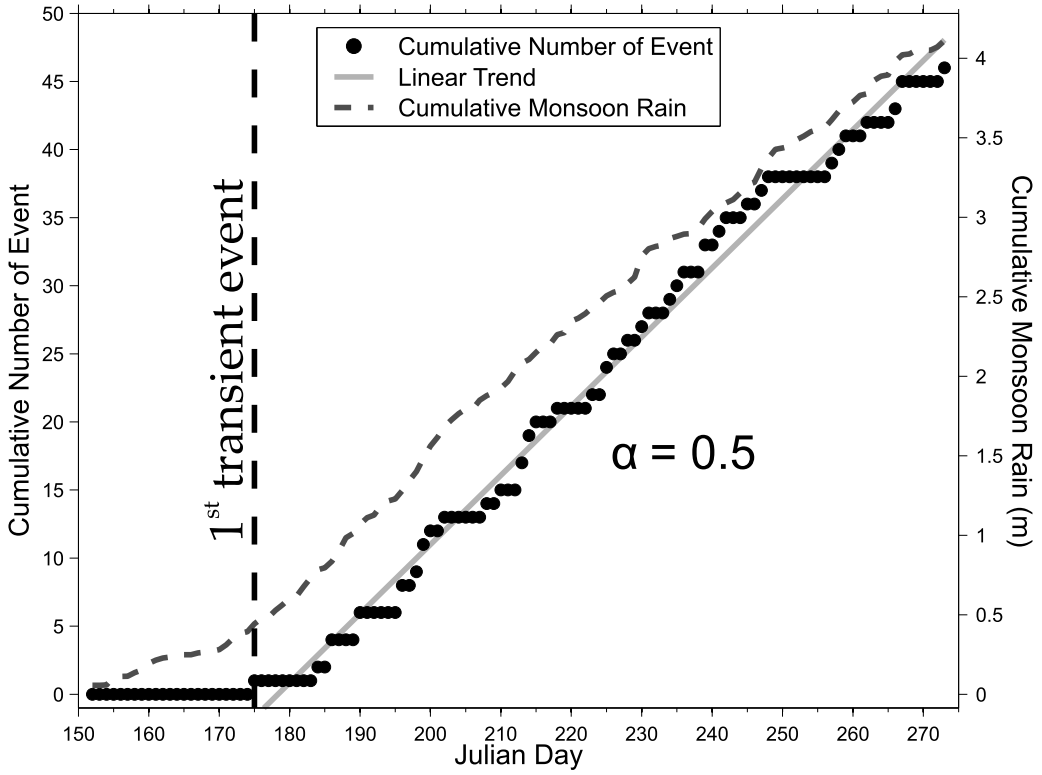

Figure 11. Cumulative number of transient events detected at H0410 (black dots) and cumulative monsoon rain (grey dashed curve) during the 2003 monsoon season. The first observed transient event seems to coincide with a slope break in the accumulated monsoon rainfall (increased daily rainfall). After this first transient event, their triggering follows a linear trend with a probability of occurrence of one event per day of 50%. The constancy of this rate during the monsoon period is coherent with the action of the accumulated monsoon rain threshold.

gullies may be responsible for intensive stream incision and toe erosion of banks. These processes, which alter the stability of slopes, may trigger debris avalanches that are channelized into gullies to form debris flows. Such successive events are generally called complex slides [*Varnes*, 1978] and have been reported along the Himalayan Arc [*Thouret*, 1983; *Paul et al.*, 2000]. Another risk associated with bed load transport in gullies is the formation of natural dams that may evolve into debris flows after their rupture. Hypothetically, such sequences of events may have resulted in the initiation of the Ramche Debris Flow and may have caused the three main peaks of energy we coherently observed on many seismic recordings (referred as P1, P2, and P3; Figure 4).

6. Conclusions

[26] The spectral analysis of the continuous seismic signals from the Hi-CLIMB stations located at the front of the Himalayan arc shows the occurrences of transient events of high-frequency seismic noise during the 2003 monsoon season. Some of these events were recorded by as many as 14 seismic stations over distances of 35 km. Their pulsatory nature lasts several hours to a few days before a total dissipation of seismic energy and a return back to a regular level of seismic noise. The transients of seismic energy over the 2–22 Hz frequency band are commonly observed in the evening and at night, a temporal feature notably associated with Himalayan rainfall during the monsoon season. The frequency characteristics observed at seismic stations in the vicinity of large landslide scars and gullies lead us to associate these transient seismic events with debris flows and intense bed load transport in the gullies. The amount of precipitation at the front of the High Range brings enough runoff to create hydrodynamics conditions sufficient to transport a wide range size of materials. This sediment is then transmitted to major river systems and could explain the pulses of suspended sediment load inferred in Nepal to be associated with mass movement activity.

[27] The complexity of the RDF slope failure is clearly seen with a detailed analysis of the seismic signals, which shows the occurrence of three major debris flows within 1 h. Their relocation using a seismic-based method reveals consistent results since they are all localized along the gullies close to H0390. However, it is difficult to conclude if the three peaks are all connected to the RDF or if some are due to other debris flow occurring along these gullies. In spite of a suboptimal array geometry for detecting the location of mass movements, our analysis shows the potential to monitor the occurrences of mass movements in space and time. Geotechnical studies coupled with detailed spectral analyses of the high-frequency seismic noise may

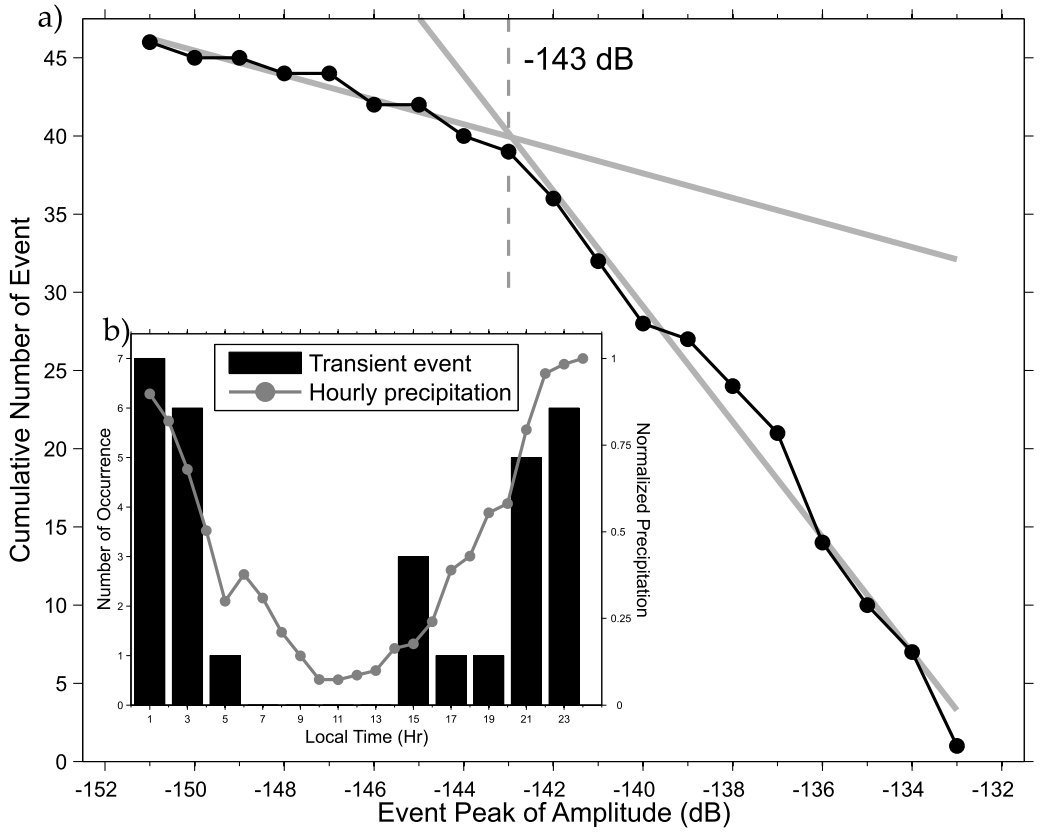

Figure 12. (a) Cumulative number of event as a function of their peak of amplitude. (b) Comparison between the temporal feature of monsoon rainfall from *Ueno et al.* [2001] and the number of transient events during the day, detected above a noise threshold of −143 dB determined in Figure 12a.

help to interpret the dynamics of the often complex slide events recorded in regions of steep slopes. The use of dedicated seismic networks may be an important tool for developing detection systems and to alert rescue missions. Furthermore, the continuous recording of transient events that may indicate a debris flow is an interesting application for risk assessments. Constraining these parameters and phenomena will help to improve our knowledge of the temporal occurrence and time structure of debris flows.

[28] Finally, the present study reveals the significant role played by gully structures as major sources of bed load transport when transients of high-frequency seismic noise are observed. Like major landslides, these events are important agents of hillslope denudation and should be considered as many sediment inputs in river systems. Future work coupling actual sediment flux measurements and seismic monitoring of debris flows could allow the emergence of a relation between the magnitude of seismic signals and eroded volumes from debris flows. This approach would lead to seismically measure denudation rates and their short-term variabilities.

Appendix A: Meteorological Data

[29] Here we use the rainfall measurements from three meteorological stations. These stations, operated by the Department of Hydrology and Meteorology of Nepal, are all located along the Trisuli valley, in the frontal part the Himalayas (Figure 1). The recorded daily rainfall exhibits large variability. The data set shows days with no reported rainfall at a station when both others record precipitation values over 50 mm (Figure S3 of the auxiliary material). Such variability cannot only be explained by a gradient of precipitation due to the high topography. Generally, ridges have rainfall 10 to 20% greater than the nearby valleys [*Craddock et al.*, 2007]. The high variations may suggest difficulties in data collection, especially during strong rainfall. Following such an argument, days with regular precipitation are expected to have a small variability whereas days with large rainfall are likely to be underestimated. To overcome this bias, we have retained only the maximum value of the daily precipitation reported by the three stations.

[30] **Acknowledgments.** The authors would like to thank the entire Hi-CLIMB team for the fieldwork and data acquisition, in particular S. Sapkota and his colleagues from the Department of Mines and Geology of Nepal. We are grateful to the Department of Hydrology and Meteorology of Nepal for providing the meteorological data. We thank B. McArdell, E. Gabet, and two anonymous reviewers for their valuable comments and suggestions on the manuscript. Project Hi-CLIMB is supported by the U.S. NSF Continental Dynamics Program, EAR 9909609.

References

Adhikari, D. P., and S. Koshimizu (2005), Debris flow disaster at Larcha, upper Bhotekoshi Valley, central Nepal, *Island Arc*, *14*(4), 410–423, doi:10.1111/j.1440-1738.2005.00495.x.

Angeli, M. G., A. Pasuto, and S. Silvano (2000), A critical review of landslide monitoring experiences, *Bull. Assoc. Eng. Geol.*, *55*(3), 133–147, doi:10.1016/S0013-7952(99)00122-2.

Arattano, M., and L. Marchi (2008), Systems and sensors for debris-flow monitoring and warning, *Sensors*, *8*, 2436–2452.

Attal, M., and J. Lavé (2006), Changes of bedload characteristics along the Marsyandi River (central Nepal): Implications for understanding hillslope sediment supply, sediment load evolution along fluvial networks, and denudation in active orogenic belts, edited by S. D. Willett et al., *Spec. Pap. Geol. Soc. Am.*, *398*, 143–171, doi:10.1130/2006.2398(09).

Barros, A. P., M. Joshi, J. Putkonen, and D. W. Burbank (2000), A study of the 1999 monsoon rainfall in a mountainous region in central Nepal using TRMM products and rain gauge observations, *Geophys. Res. Lett.*, *27*(22), 3683–3686.

Bollasina, M., L. Bertolani, and G. Tartari (2002), Meteorological observations at high altitude in the Khumbu Valley, Nepal Himalayas, 1994–1999, *Bull. Glaciol. Res.*, *19*, 1–11.

Brardinoni, F., O. Slaymaker, and M. A. Hassan (2003), Landslide inventory in a rugged forested watershed: A comparison between air-photo and field survey data, *Geomorphology*, *54*(3–4), 179–196, doi:10.1016/S0169-555X(02)00355-0.

Burbank, D. W., J. Leland, E. Fielding, R. S. Anderson, N. Brozovic, M. R. Reid, and C. Duncan (1996), Bedrock incision, rock uplift and threshold hillslopes in the northwestern Himalayas, *Nature*, *379*, 505–510, doi:10.1038/379505a0.

Burtin, A., L. Bollinger, J. Vergne, R. Cattin, and J. L. Nábělek (2008), Spectral analysis of seismic noise induced by rivers: A new tool to monitor spatiotemporal changes in stream hydrodynamics, *J. Geophys. Res.*, *113*, B05301, doi:10.1029/2007JB005034.

Craddock, W. H., D. W. Burbank, B. Bookhagen, and E. J. Gabet (2007), Bedrock channel geometry along an orographic rainfall gradient in the upper Marsyandi River valley in central Nepal, *J. Geophys. Res.*, *112*, F03007, doi:10.1029/2006JF000589.

Dahal, R. K., and S. Hasegawa (2008), Representative rainfall thresholds for landslides in the Nepal Himalaya, *Geomorphology*, *100*(3–4), 429–443, doi:10.1016/j.geomorph.2008.01.014.

Dhital, M. R. (2003), Causes and consequences of the 1993 debris flows and landslides in the Kulekhani watershed, central Nepal, in *Debris-Flow Hazards Mitigation: Mechanics, Prediction and Assessment*, pp. 931–942, Rotterdam Millpress, Davos, Switzerland.

Dhital, M. R., B. N. Upreti, V. Dangol, A. N. Bhandari, and A. Bhattarai (1991), Engineering geological methods applied in mountain road survey: An example from Baitadi-Darchula road project (Nepal), *J. Nepal Geol. Soc.*, *7*, 49–67.

du Boys, M. P. (1879), Étude du régime du Rhône et de l'action exercée par les eaux sur un lit à fond de graviers indéfiniment affouillable, *Ann. Ponts Chaussées*, *18*(5), 141–195.

Gabet, E. J., D. W. Burbank, J. K. Putkonen, B. A. Pratt-Sitaula, and T. Ojhac (2004), Rainfall thresholds for landsliding in the Himalayas of Nepal, *Geomorphology*, *63*(3–4), 131–143, doi:10.1016/j.geomorph.2004.03.011.

Gabet, E. J., D. W. Burbank, B. Pratt-Sitaula, J. Putkonen, and B. Bookhagen (2008), Modern erosion rates in the High Himalayas of Nepal, *Earth Planet. Sci. Lett.*, *267*(3–4), 482–494, doi:10.1016/j.epsl.2007.11.059.

Hasegawa, S., R. K. Dahal, M. Yamanaka, N. P. Bhandary, R. Yatabe, and H. Inagaki (2008), Causes of large-scale landslides in the Lesser Himalaya of central Nepal, *Environ. Geol.*, *57*, 1423–1434, doi:10.1007/s00254-008-1420-z.

Hetényi, G. (2007), Evolution of deformation of the Himalayan prism: From imaging to modelling, Ph.D. thesis, Univ. Paris-Sud XI, 400 pp.

Hovius, N., C. P. Stark, C. Hao-Tsu, and L. Jiun-Chuan (2000), Supply and removal of sediment in a landslide-dominated mountain belt: Central Range, Taiwan, *J. Geol.*, *108*(1), 73–89, doi:10.1086/314387.

Huang, C.-J., H.-Y. Yin, C.-Y. Chen, C.-H. Yeh, and C.-L. Wang (2007), Ground vibrations produced by rock motions and debris flows, *J. Geophys. Res.*, *112*, F02014, doi:10.1029/2005JF000437.

Itakura, Y., H. Inaba, and T. Sawada (2005), A debris-flow monitoring devices and methods bibliography, *Nat. Hazards Earth Syst. Sci.*, *5*(6), 971–977.

Iverson, R. M., M. E. Reid, and L. R. G. (1997), Debris flow mobilization from landslides, *Annu. Rev. Earth Planet. Sci.*, *25*, 85–138, doi:10.1146/annurev.earth.25.1.85.

Kathmandu Post (2003), Landslides claim 15 soldiers, one civilian, p. 1, 17 August.

Lavé, J., and J.-P. Avouac (2001), Fluvial incision and tectonic uplift across the Himalayas of central Nepal, *J. Geophys. Res.*, *106*(B11), 26,561–26,592.

Malet, J. P., O. Maquaire, and E. Calais (2002), The use of Global Positioning System techniques for the continuous monitoring of landslides: Application to the Super-Sauze earthflow (Alpes-de-Haute-Provence, France), *Geomorphology*, *43*(1–2), 33–54, doi:10.1016/S0169-555X(01)00098-8.

Marchi, L., M. Arattano, and A. M. Deganutti (2002), Ten years of debris-flow monitoring in the Moscardo Torrent (Italian Alps), *Geomorphology*, *46*(1–2), 1–17, doi:10.1016/S0169-555X(01)00162-3.

Marston, R. A., M. M. Miller, and L. P. Devkota (1998), Geoecology and mass movement in the Manaslu-Ganesh and Langtang-Jugal Himals, Nepal, *Geomorphology*, *26*(1–3), 139–150, doi:10.1016/S0169-555X(98)00055-5.

Nábělek, J., G. Hetényi, J. Vergne, S. Sapkota, B. Kafle, M. Jiang, H. Su, J. Chen, B.-S. Huang, and the Hi-CLIMB Team (2009), Underplating in the Himalaya-Tibet collision zone revealed by the Hi-CLIMB experiment, *Science*, *325*, 1371–1374, 10.1126/science.1167719.

Paul, S. K., S. K. Bartarya, P. Rautela, and A. K. Mahajan (2000), Catastrophic mass movement of 1998 monsoons at Malpa in Kali Valley, Kumaun Himalaya (India), *Geomorphology*, *35*(3–4), 169–180, doi:10.1016/S0169-555X(00)00032-5.

Percival, D. B., and A. T. Walden (1993), *Spectral Analysis for Physical Applications: Multitaper and Conventional Univariate Techniques*, Cambridge Univ. Press, Cambridge, U. K.

Reid, L. M. (1998), Calculation of average landslide frequency using climatic records, *Water Resour. Res.*, *34*(4), 869–877.

Shields, A. (1936), Anwendung der Aehnlichkeitsmechanik und der Turbulenzforschung auf die Geschiebebewegung, *Mitt. Preuss. Versuchsanst. Wasserbau Schiffbau*, *26*, 1–26. (*Hydrodyn. Lab. Publ.*, Engl. Transl., *167*.)

Shrestha, S. B., J. N. Shrestha, and S. R. Sharma (1985), Geological map of central Nepal, scale 1:250.000, Dep. of Mines and Geol., Kathmandu.

Shroder, J. F. (1998), Slope failure and denudation in the western Himalaya, *Geomorphology*, *26*(1–2), 81–105, doi:10.1016/S0169-555X(98)00052-X.

Thomson, D. J. (1982), Spectrum estimation and harmonic analysis, *Proc. IEEE*, *70*(9), 1055–1096.

Thouret, J. C. (1983), Field research on slopes evolution in the Himalaya range: the example of the Ankhu Khola valley, central Nepal, in *Géodynamique des Grands Versants de l'Ankhu Khola, Népal Central*, p. 231, Cent. Natl. de la Rech. Sci., Paris.

Ueno, K., et al. (2001), Meteorological observations during 1994–2000 at the Automatic Weather Station (GEN-AWS) in Khumbu region, Nepal Himalayas, *Bull. Glaciol. Res.*, *18*, 23–30.

Upreti, B. N. (1999), An overview of the stratigraphy and tectonics of the Nepal Himalaya, *J. Asian Earth Sci.*, *17*(5), 577–606, doi:10.1016/S1367-9120(99)00047-4.

Upreti, B. N., and M. R. Dhital (1996), *Landslide Studies and Management in Nepal*, 87 pp., Int. Cent. for Integrated Mt. Dev., Kathmandu.

Varnes, D. J. (1978), Slope movements and types and processes, *Landslides: Analysis and Control. Special Report 176, Transport Research Board*, pp. 11–33, Natl. Acad. of Sci., Washington D. C.

Zhang, S., Y. Hong, and B. Yu (2004), Detecting infrasound emission of debris flows for warning purposes, paper presented at 10th Congress, INTERPRAEVENT, Riva del Garda, Trento, Italy, 24–27 May.

L. Bollinger, CEA, DAM, DIF, F-91297 Arpajon CEDEX, France.

A. Burtin, Laboratoire de Géologie, École Normale Supérieure de Paris, CNRS, 24 rue Lhomond, F-75231 Paris CEDEX 05, France. (burtin@geologie.ens.fr)

R. Cattin, Géosciences Montpellier, Université Montpellier 2, CNRS, F-34095 Montpellier, France.

J. L. Nábělek, College of Oceanic and Atmospheric Sciences, Oregon State University, Corvallis, OR 97331, USA.

J. Vergne, Institut de Physique du Globe de Strasbourg, UMR 7516, CNRS-ULP, F-67084 Strasbourg, France.